Sub-barrier fusion enhancement caused by positive Q-value four-neutron transfer*

Ning Wang (王宁)[1][†] [ID]   Yi-Jie Duan (段异婕)[1]   Hong Yao (姚红)[1][‡]   Hui-Ming Jia (贾会明)[2] [ID]

[1]Guangxi Key Laboratory of Nuclear Physics and Technology, Guangxi Normal University, Guilin 541004, China
[2]Department of Nuclear Physics, China Institute of Atomic Energy, Beijing 102413, China

Abstract: The effect of positive Q-value four-neutron transfer (PQ4NT) on the sub-barrier capture cross sections is investigated systematically using the empirical barrier distribution (EBD2) method. For 13 fusion reactions with $Q_{4n} > 0$, the sustained neutron-pair transfer reduces barrier heights and enhances capture cross sections at sub-barrier energies. In contrast, reactions such as $^{18}O+^{58}Ni$, which have $Q_{2n} > 0$ and $Q_{4n} < 0$, exhibit no enhancement due to stalling of subsequent neutron-pair transfer after the initial 2n transfer. Incorporating PQ4NT effects into EBD2 for systems with $Q_{4n} > 0$ significantly reduces the average deviation between the predicted and experimental capture cross sections (113 datasets) by 20%. In comparison with those in reactions induced by ^{48}Ca ($Q_{4n} < 0$), the neutron pickup probabilities in the quasi-elastic scattering of ^{40}Ca-induced reactions ($Q_{4n} > 0$) are considerably larger, according to the time-dependent Hartree-Fock calculations.

Keywords: heavy-ion fusion, barrier distribution, neutron transfer, cross-section enhancement

I. INTRODUCTION

The sub-barrier fusion of heavy-ions [1−10] is a crucial process for understanding nuclear structure effects and quantum many-body dynamics in nuclei [11−14], and it exhibits complex behavior influenced by couplings to internal degrees of freedom [15, 16]. Among these couplings, the role of positive Q-value neutron transfer (PQNT) channels remains a contentious topic in nuclear physics [17−27]. While significant sub-barrier fusion enhancement attributed to positive Q-value neutron transfer has been proposed in systems such as $^{40}Ca+^{94,96}Zr$ [23], recent high-precision measurements for $^{18}O+^{58}Ni$ reveal no such enhancement [27] despite a large positive Q-value for two-neutron transfer ($Q_{2n} = +8.20$ MeV). This apparent contradiction underscores the need to identify the precise conditions governing the effect of PQNT.

The current understanding suggests that PQNT enhances sub-barrier fusion through mechanisms such as neutron-rich neck formation [28, 29], which reduces the effective fusion barrier or increases nuclear deformation. Significant deformation increases after neutron transfer correlate with fusion enhancement, while minimal deformation change results in negligible effects [17, 20]. However, the calculated nuclear deformation is model-dependent (*e.g.*, FRDM model [30] predicts $\beta_2 = 0.217$ for ^{96}Zr while WS4 [31] suggests near-sphericity), resulting in uncertainty in analysis and predictions. Rachkov *et al.* emphasized that a positive Q-value is necessary but insufficient, highlighting the importance of nuclear "rigidity" (resistance to collective excitations) and limiting significant influence to 1n and 2n transfers [19].

A critical yet unexplored factor may be the continuity of neutron transfer feasibility. Positive Q-values for initial transfers (*e.g.*, 2n) may not suffice if subsequent transfers are energetically forbidden. For example, in $^{40}Ca+^{96}Zr$, the Q-values $Q_{2n} = +5.53$ MeV and $Q_{4n} = +9.64$ MeV are favorable for sustained transfer, and the enhancement is observed. For $^{18}O+^{58}Ni$, $Q_{2n} = +8.20$ MeV; however, $Q_{4n} = -2.27$ MeV. This implies that neutron transfer stalls after 2n and no enhancement occurs. Thus, the sign and magnitude of Q-values for multi-neutron transfers (particularly 4n) can determine if neutron neck formation persists, influencing barrier lowering. While the effect of 1n and 2n transfers has been studied extensively, that of positive Q-value four-neutron (4n) transfer on sub-barrier fusion dynamics remains systematically unaddressed.

This work aims to bridge this gap by investigating the role of 4n transfer Q-values in sub-barrier fusion en-

---

hancement. We analyze systematics across diverse reaction systems to explore correlations between the sign of Q_{4n} and fusion enhancement. By integrating the continuity of neutron-pair transfer and nuclear rigidity, we seek to establish predictive criteria for the occurrence of the effect of PQNT. Recently, Wang proposed an analytical formula (EBD2) [32] with high accuracy for a systematic description of the capture cross sections at near-barrier energies from light to superheavy reaction systems based on the empirical barrier distribution (EBD) method [33, 34]. In EBD2, the effect of PQNT is not yet involved. Therefore, it is interesting to investigate the effect of PQNT using EBD2 predictions as reference. The remainder of this paper is organized as follows. In Sec. II, the framework of the EBD2 formula and the correction terms owing to positive Q-value four-neutron transfer (PQ4NT) are introduced. In Sec. III, the results from the proposed formula for a series of reaction systems and some discussions are presented. Finally a summary is given in Sec. IV.

II. EMPIRICAL BARRIER DISTRIBUTION FORMULA

In this work, the capture cross section is written as [32]

$$\sigma_{\text{cap}}(E_{\text{c.m.}}) = \pi R_B^2 \frac{W}{\sqrt{2}E_{\text{c.m.}}} \left[X\text{erfc}(-X) + \frac{1}{\sqrt{\pi}} \exp(-X^2) \right],$$
(1)

where $X = \dfrac{E_{\text{c.m.}} - V_B}{\sqrt{2}W}$. $E_{\text{c.m.}}$ represents the center-of-mass incident energy; V_B and W represent the centroid and standard deviation of the Gaussian function, respectively; and R_B is the barrier radius. The average barrier height V_B (in MeV) is parameterized as

$$V_B = 1.051z + 0.000335z^2 + \Delta B - \Delta_{\text{tr}}.$$
(2)

z denotes the Coulomb parameter

$$z = \frac{Z_1 Z_2}{A_1^{1/3} + A_2^{1/3}} F_S$$
(3)

with $F_S = 1 - Z_1^{-1/3} Z_2^{-1/3}$. Z_1 and Z_2 represent the charge numbers of the projectile nucleus and target, respectively. A_1 and A_2 represent the corresponding mass numbers of the reaction partners. The correction term $\Delta B = \sum \Delta_i I_i^2$ in Eq. (2) considers the competition between shell and isospin effects, with the shell gap Δ_i [35] and isospin asymmetry $I_i = (N_i - Z_i)/A_i$ of the reaction partners ($i = 1$ for projectile and $i = 2$ for target). In this new version of the EBD (v2.2) formula, an additional correction term

$\Delta_{\text{tr}} = Q_{4n}|I_1 - I_2|/2$ is introduced for reactions with $Q_{4n} > 0$ to consider the effect of PQ4NT on barrier height. Here, $|I_1 - I_2|/2$ considers the isospin diffusion between the reaction partners. Q_{4n} represents the Q-value for 4n transfer, providing additional energy to transfer neutron pairs. It is expressed as $Q_{4n} = \max(Q_{4n}^+, Q_{4n}^-)$ based on the masses of reaction partners.

$$Q_{4n}^+ = M(A_1, Z_1) + M(A_2, Z_2) - M(A_1 + 4, Z_1) - M(A_2 - 4, Z_2),$$
(4)

$$Q_{4n}^- = M(A_1, Z_1) + M(A_2, Z_2) - M(A_1 - 4, Z_1) - M(A_2 + 4, Z_2).$$
(5)

Considering that Δ_{tr} should be a small correction to the barrier height, we introduce a truncation, *i.e.*, $\Delta_{\text{tr}} \leqslant 1$ MeV, for systems with extremely large values of Q_{4n}.

The standard deviation of the Gaussian function is parameterized as [32]

$$W = c_0(1 + w_d) + c_1 V_B \sqrt{w_1^2 + w_2^2 + w_0^2} - \Delta B/N_{\text{CN}}^{1/3} + g\Delta_{\text{tr}}, \quad (6)$$

where $w_d = \sum |\beta_{2i}| A_i^{1/3}$ and $w_i = A_i^{1/3}\beta_{2i}^2/(4\pi)$, with the mass numbers A_1 and A_2 of the reaction partners and their quadrupole deformation parameters β_2 taken from the WS4 model [31] for prolate nuclei heavier than ^{16}O. $w_0 = (V_B + Q)/c_2$ is introduced to consider the dynamical effects caused by the excitation energy at the capture position, which is approximately proportional to the excitation energy of a compound nucleus. Q represents the reaction Q-value in the fusion process from the ground states of the projectile and target nuclei to that of the compound nucleus. Further, N_{CN} represents the neutron number of the compound nucleus. The values of model parameters $c_0 = 0.63$ MeV, $c_1 = 0.015$, and $c_2 = 33.0$ MeV are the same as those adopted in the previous version [32]. The last term in Eq. (6) considers the effect of PQ4NT on barrier distribution. The factor $g = \langle S_{2n} \rangle/(V_B + Q)$ considers the effect of nuclear "rigidity." $\langle S_{2n} \rangle$ represents the average two-neutron separation energy of the di-nuclear system. In particular, $\langle S_{2n} \rangle = [S_{2n}(A_2, Z_2) + S_{2n}(A_1 + 2, Z_1)]/2$ if the isospin asymmetry $I_2 > I_1$; otherwise, we set $\langle S_{2n} \rangle = [S_{2n}(A_1, Z_1) + S_{2n}(A_2 + 2, Z_2)]/2$. The contribution of Δ_{tr} is relatively larger for the fusion reactions with low excitability (*i.e.*, with smaller excitation energy at capture position), which is consistent with the conclusion in [19]. Thus, the "rigidity" of colliding nuclei with respect to collective excitation is important for sub-barrier fusion enhancement. For fusion reactions with light nuclei such as ^{4}He, ^{12}C, and ^{16}O, the nuclear deformation effects on the capture cross sections are weakened because of the large de Broglie

wavelength. In this work, the value of W is written as

$$W = c_0 + c_1 V_B \qquad (7)$$

for light nuclei ($A \leqslant 16$) induced reactions with $\lambdabar_B \geqslant 0.18$ fm. Here, $\lambdabar_B = \hbar / \sqrt{2\mu V_B}$ indicates the reduced de Broglie wavelength of the colliding nuclei at an incident energy of $E_{\text{c.m.}} = V_B$. μ is the reduced mass of the reaction system.

III. RESULTS AND DISCUSSIONS

A. Capture cross sections

We first investigate the discrepancies between the EBD2 predictions and measured capture cross sections for ^{154}Sm and ^{116}Sn involved fusion reactions. We focus on medium-mass reaction systems in which the quasi-fission is negligible and the capture excitation function is therefore approximately equal to the corresponding fusion excitation function. The barrier parameters for some fusion reactions and the corresponding values of Q_{4n} and Q_{2n} are listed in Table 1, wherein the barrier height V_B is

obtained through Eq. (2), the values of W are given by Eq. (6), and the barrier radii R_B are taken from Eq. (4) in [32]. For ^{48}Ca+^{154}Sm, ^{48}Ca+^{208}Pb, and ^{40}Ca + ^{90}Zr, both Q_{2n} and Q_{4n} are negative. For ^{18}O+^{58}Ni and ^{18}O+^{116}Sn, $Q_{2n} > 0$ and $Q_{4n} < 0$. For other reactions in the table, both Q_{2n} and Q_{4n} are positive. In Fig. 1, we show the capture excitation functions for ^{16}O+^{154}Sm [6], ^{48}Ca+^{154}Sm [36], ^{18}O+^{116}Sn [26], ^{28}Si+^{154}Sm [37], ^{32}S+^{154}Sm [38], and ^{32}S+^{116}Sn [39]. For the three reactions ^{16}O+^{154}Sm, ^{48}Ca+^{154}Sm, and ^{18}O+^{116}Sn, the corresponding values of Q_{4n} are negative. For the other three reactions, $Q_{4n} > 0$, $i.e.$, the Q values are favorable for sustained neutron transfer. One can see from the figure that, for reactions with $Q_{4n} < 0$, the experimental data can be reproduced remarkably well by the EBD2. For the reactions with $Q_{4n} > 0$, the capture cross sections at sub-barrier energies are slightly under-predicted, which could be caused by the neutron transfer effects not being involved in the EBD2 calculations.

For further verifying the correlation between the effect of PQ4NT and the sub-barrier enhancement of capture cross sections, we systematically compare the dis-

Table 1. Barrier parameters adopted in EBD2.2 for some fusion reactions. Here, Q_{4n} and Q_{2n} represent the corresponding Q-values for 4n and 2n transfers, respectively.

| Reaction	V_B /MeV	R_B /fm	W/MeV	Q_{4n} /MeV	Q_{2n} /MeV
^{18}O+^{58}Ni	30.69	8.54	1.44	-2.27	+8.20
^{18}O+^{116}Sn	49.40	9.52	1.89	-9.22	+4.08
^{28}Si+^{154}Sm	99.54	10.10	3.96	+7.18	+5.25
^{32}S +^{154}Sm	112.79	10.09	4.42	+9.25	+6.23
^{40}Ca+^{154}Sm	139.23	9.84	5.30	+11.22	+6.01
^{48}Ca+^{154}Sm	137.12	10.45	4.27	-5.37	-2.33
^{28}Si+^{208}Pb	126.16	10.42	2.88	+5.95	+4.98
^{32}S+^{208}Pb	143.11	10.21	3.37	+8.01	+5.95
^{36}Ar+^{208}Pb	160.15	9.83	3.85	+8.17	+6.52
^{40}Ca+^{208}Pb	176.97	9.25	4.14	+9.98	+5.74
^{48}Ca+^{208}Pb	174.16	10.38	2.10	-6.60	-2.60
^{44}Ti+^{208}Pb	193.84	8.46	4.83	+14.30	+8.62
^{32}S+^{94}Zr	78.42	9.50	2.54	+6.15	+5.11
^{32}S+^{96}Zr	78.00	9.55	2.67	+7.66	+5.74
^{32}S+^{104}Ru	85.11	9.62	3.04	+5.78	+4.93
^{32}S+^{116}Sn	95.80	9.71	2.88	+1.78	+2.95
^{32}S+^{182}W	131.85	10.10	4.06	+6.81	+5.31
^{40}Ca+^{90}Zr	97.79	9.48	2.45	-4.18	-1.45
^{40}Ca+^{94}Zr	96.33	9.59	3.06	+8.13	+4.89
^{40}Ca+^{96}Zr	95.83	9.65	3.25	+9.64	+5.53
^{40}Ca+^{124}Sn	115.68	9.88	3.85	+9.49	+5.41
^{40}Ca+^{132}Sn	114.79	10.08	4.00	+13.44	+7.29

crepancies between the calculated barrier heights with EBD2 and 382 datasets of extracted values for fusion reactions induced by nuclei with $A \geqslant 12$ [40]. Simultaneously, deviations between the predicted capture cross sections with EBD2 and 426 datasets of measured cross sections [34] are explored systematically. In Fig. 2, we show the distributions of the deviations of the barrier heights and capture cross sections. The blue and red bars represent the results for cases with $Q_{4n} < 0$ and those with $Q_{4n} > 0$, respectively. We observe that, for reactions with $Q_{4n} > 0$, both the discrepancies in barrier heights and deviations in capture cross sections are systematically larger compared with those of the $Q_{4n} < 0$ cases. Although the average mean-square deviation is 0.111 for the reac-

tions with $Q_{4n} < 0$, the deviation goes up to 0.118 for the cases with $Q_{4n} > 0$, which indicates that the neutron transfer effects are not negligible for the fusion reactions with $Q_{4n} > 0$.
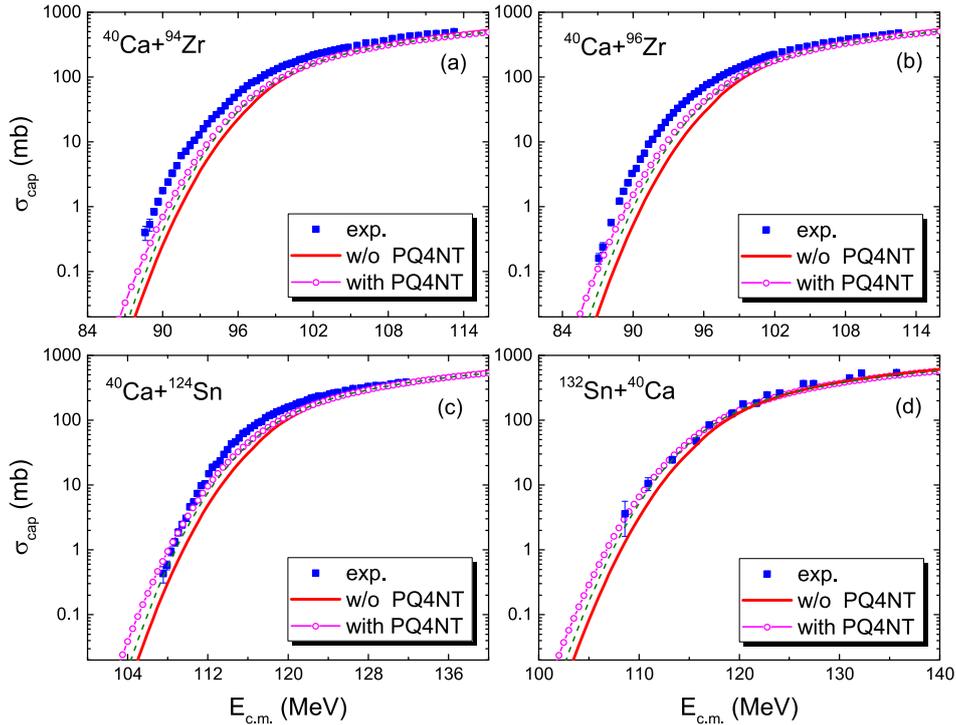
In Fig. 3, we show the capture excitation functions for four fusion reactions $^{40}Ca + {}^{94}Zr$, $^{40}Ca + {}^{96}Zr$, $^{40}Ca + {}^{124}Sn$, and $^{132}Sn + {}^{40}Ca$ with $Q_{4n} > 0$. The circles and solid curves represent the results with and without considering the effect of PQ4NT, respectively. The experimental data can be better reproduced by considering the effect of PQ4NT in EBD2 calculations, *i.e.*, when the Δ_{tr} terms are involved. The values of Q_{4n} for these reactions are listed in Table 1. For the reactions with $Q_{4n} > 0$, the corresponding Q-values for two-neutron transfer are also posit-
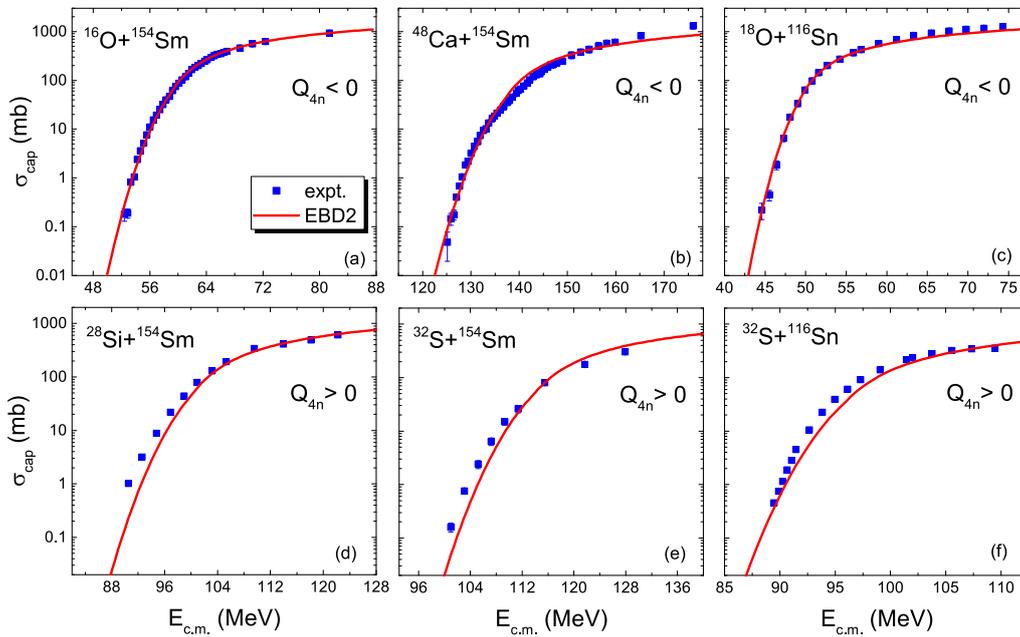
Fig. 1. (color online) Capture excitation functions for $^{16}O + {}^{154}Sm$ [6], $^{48}Ca + {}^{154}Sm$ [36], $^{18}O + {}^{116}Sn$ [26], $^{28}Si + {}^{154}Sm$ [37], $^{32}S + {}^{154}Sm$ [38], and $^{32}S + {}^{116}Sn$ [39]. The squares and curves denote the experimental data and predictions of EBD2 [32], respectively.
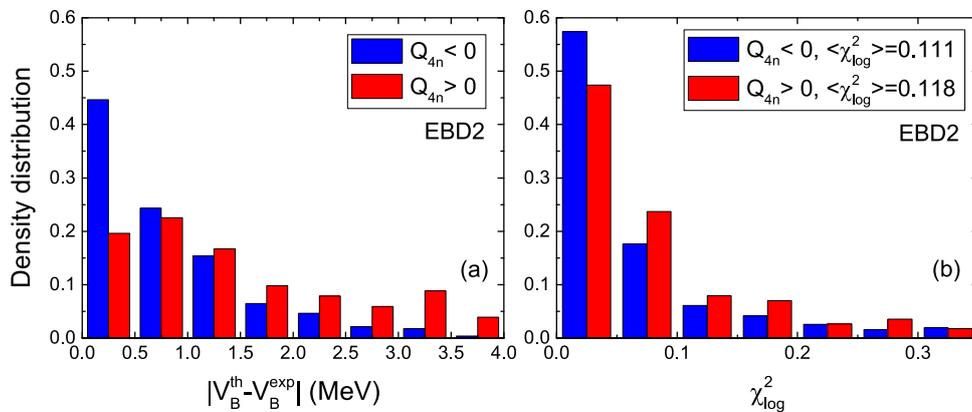
Fig. 2. (color online) (a) Distribution of the discrepancies between the calculated barrier heights V_B^{th} with EBD2 and extracted ones V_B^{exp} [40]. (b) Distribution of the mean-square deviation between the predicted cross-sections with EBD2 and the experimental data in logarithmic scale. The blue and red bars denote the results for the cases with $Q_{4n} < 0$ and $Q_{4n} > 0$, respectively.

Fig. 3. (color online) Capture excitation functions for reactions ^{40}Ca + ^{94}Zr [41], ^{40}Ca + ^{96}Zr [42], ^{40}Ca + ^{124}Sn [43], and ^{132}Sn + ^{40}Ca [44]. The squares denote the experimental data. The solid curves and circles represent the results of EBD2 and those with the PQ4NT effect being considered in the calculations, respectively. The dashed curves represent the results obtained considering the Δ_{tr} term in Eq. (2) and neglecting the Δ_{tr} term in Eq. (6).

ive. For ^{40}Ca + ^{94}Zr and ^{40}Ca + ^{96}Zr, the values of Q_{4n} are 8.13 MeV and 9.64 MeV, respectively. This implies that the subsequent neutron-pair transfers are energetically favorable and the enhancements are clearly observed. Considering the effect of PQ4NT in the calculations, the results are evidently improved; however, the under-prediction of the experimental data still exists. To see the contribution of the Δ_{tr} term in W, we present the results (dashed curves) neglecting the Δ_{tr} term of W in the calculations. The sub-barrier capture cross sections can be further enhanced by considering the Δ_{tr} term of W. The average deviation between the predicted results and 113 datasets of measured cross sections [32] can be further reduced by 6%. Among all the reactions considered in this work, there are only six reactions ^{40}Ca+^{192}Os, ^{40}Ca+^{208}Pb, ^{40}Ca+^{238}U, ^{132}Sn+^{40}Ca, ^{132}Sn+^{58}Ni, and ^{134}Te+^{40}Ca with $\Delta_{\text{tr}} > 1$ MeV, and the truncation at 1 MeV has a minimal impact on the overall fit.

In Figs. 4 and 5, we show the corresponding comparisons for more fusion reactions with $Q_{4n} > 0$. All results are improved when the effects of PQ4NT are involved in the calculations, which indicates that PQ4NT plays an important role in the sub-barrier enhancement of the capture cross sections. By considering the effects of PQ4NT in the calculations for the reactions with $Q_{4n} > 0$, the average deviation between the predicted results and 113 datasets of measured cross sections [32] is significantly

reduced by 20% (from 0.118 to 0.094). Considering that the values of Q_{4n} are 8.17 MeV and 14.30 MeV for ^{36}Ar+^{208}Pb and ^{44}Ti+^{208}Pb (see Table 1), respectively, the sub-barrier fusion enhancement caused by a positive Q-value four-neutron transfer can be observed in these two unmeasured reactions.

B. Uncertainties of Model Predictions

We systematically investigate the uncertainty of the predicted capture cross sections with EBD2.2. A total of 426 datasets of measured cross sections [34], including the systems collected in Refs. [25, 40, 52] except those induced by nuclei lighter than ^{12}C is used. In Fig. 6(a), we show the deviations between the predicted capture cross sections σ_{th} and the experimental data σ_{exp} (in logarithmic scale) for 426 datasets of the measured cross sections. The deviations at sub-barrier energies are relatively large, and the deviations systematically decrease with increasing incident energy. To investigate the energy-dependence of the uncertainties of model predictions, we calculate the corresponding root-mean-square deviations (RMSD) at different values of $E_{\text{c.m.}}/V_B$. The squares in Fig. 6(b) show the calculated RMSD as a function of $E_{\text{c.m.}}/V_B$. As seen in Fig. 6, the RMSD are relatively larger at sub-barrier energies comparing with the above-barrier cases. At incident energies $E_{\text{c.m.}} > 0.9\,V_B$, the deviation decreases systematically with $E_{\text{c.m.}}$ and ap-
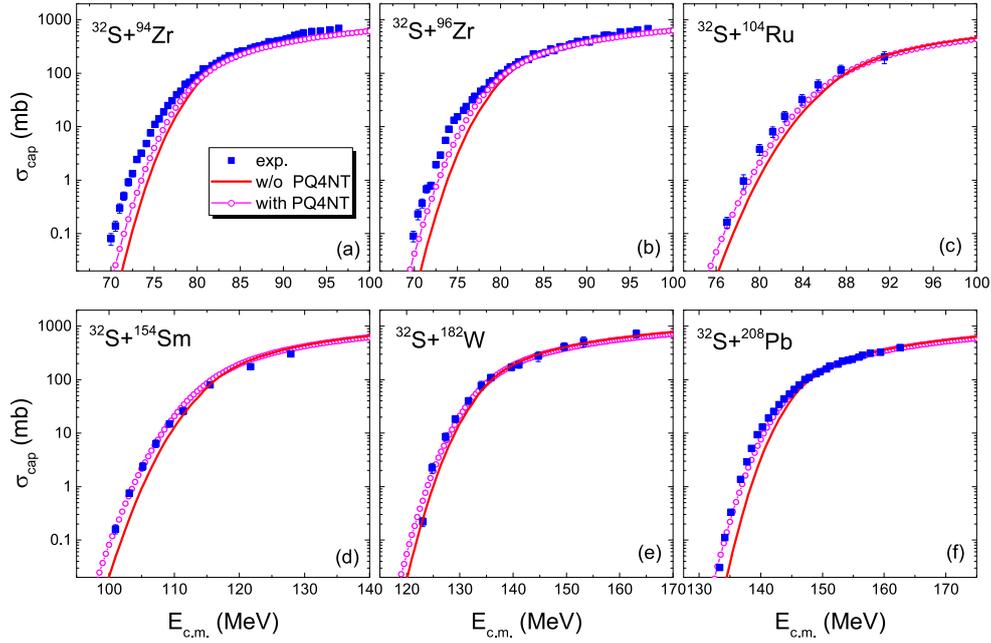
Fig. 4. (color online) Same as Fig. 3 but for reactions ^{32}S+^{94}Zr [45], ^{32}S+^{96}Zr [46], ^{32}S+^{104}Ru [47], ^{32}S+^{154}Sm [38], ^{32}S+^{182}W [48], and ^{32}S+^{208}Pb [49].
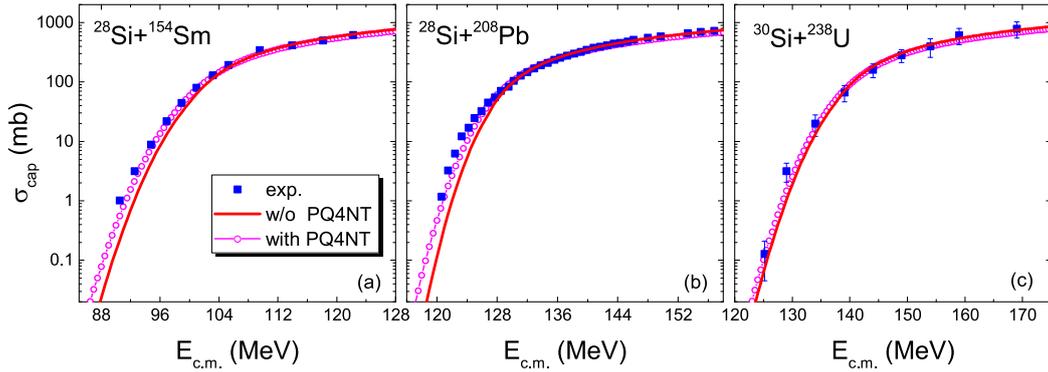
Fig. 5. (color online) Same as Fig. 3 but for reactions ^{28}Si+^{154}Sm [37], ^{28}Si+^{208}Pb [50], and ^{30}Si+^{238}U [51].

proaches ~ 0.085.

By fitting the calculated rms deviations with a Gaussian function plus a Fermi function, we obtain an energy-dependent RMSD for EBD2.2 [see the solid curve in Fig. 6(b)],

$$\mathrm{RMSD} = 0.085 + 0.20 \exp\left[-\left(\frac{E_{\mathrm{c.m.}}/V_{\mathrm{B}} - 0.92}{0.035}\right)^2\right] +$$
$$0.465\left[1 + \exp\left(\frac{E_{\mathrm{c.m.}}/V_{\mathrm{B}} - 0.97}{0.03}\right)\right]^{-1}. \quad (8)$$

Equation (8) provides an energy-dependent RMSD derived from the extensive datasets of the measured fusion reactions. This empirical RMSD can be applied to estimate the uncertainty of predictions for unmeasured systems. Figure 7 shows the predicted capture cross sections for six fusion reactions with deformed nuclei, wherein

several reactions are not included in the fitting datasets. For energies well above this barrier, the RMSD converges to approximately 0.085, which corresponds to a relative uncertainty of approximately 21.6% (*i.e.*, $\sigma_{\mathrm{th}} \times 10^{0.085} \approx 1.216\sigma_{\mathrm{th}}$). This quantitative uncertainty assessment is valuable for predicting evaporation residue cross sections in the synthesis of superheavy nuclei, where accurate extrapolations of capture cross sections are crucial [53]. To test the predictive power of EBD2.2, the measured capture excitation functions of three reactions ^{12}C+^{24}Mg [54, 55], ^{12}C+^{184}W [56], and ^{12}C+^{248}Cm [57], which are not included in the 426 datasets mentioned previously, are also presented in Fig. 7 for comparison. The shadows represent predictions of EBD2.2 with default values for the parameters. These "new" data can be reproduced reasonably well.

To investigate the effect of the de Broglie wavelength on the capture cross sections, we present the reduced de
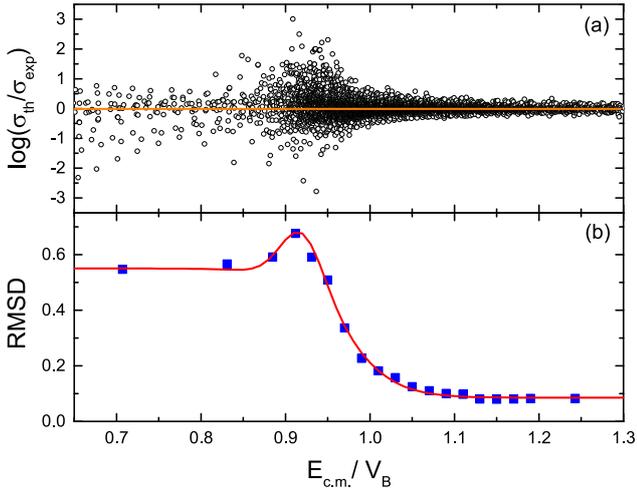
Fig. 6. (color online) (a) Deviations between predicted capture cross sections with EBD2.2 and experimental data as a function of the ratio $E_{c.m.}/V_B$. (b) Root-mean-square deviations with respect to the measured capture cross sections (in log) as a function of $E_{c.m.}/V_B$. The squares denote the calculated results with the data in (a). The solid curve denotes the results by fitting the squares.

Broglie wavelength λ_B of the colliding nuclei in Fig. 7. For ^{12}C+^{24}Mg, ^{12}C+^{154}Sm, and ^{12}C+^{184}W, the values of λ_B are larger than 0.18 fm. The experimental data for these three reactions can be well reproduced using Eq. (7) in the calculations, *i.e.*, neglecting the deformation effects.

As the de Broglie wavelength increases for light systems, the wave function of the incident nucleus spreads out, such that it is no longer sensitive to specific orientations of the deformed target nucleus; instead, it interacts with an average potential field. Consequently, the enhancement of the capture cross sections at sub-barrier energies caused by deformation weakens, and its behavior gradually approaches results calculated using spherical shapes. For heavier systems such as ^{12}C+^{248}Cm (with $\lambda_B = 0.170$ fm) and ^{16}O+^{154}Sm (with $\lambda_B = 0.156$ fm), the measured cross sections are under-predicted if the deformation effects are neglected. This indicates that the light nucleus with a de Broglie wavelength of about $\lambda_B < 0.18$ fm can "sense" the anisotropic effects caused by the orientations of the deformed target nucleus; therefore, the deformation effects cannot be neglected. In Fig. 7(f), the capture excitation functions for ^{40}Ar+^{243}Am are simultaneously predicted, in which λ_B is very small and the deformation effects influence the sub-barrier capture cross sections.

C. Physical interpretation of PQ4NT effects

The sub-barrier fusion enhancement attributed to neutron transfer was previously investigated based on the QCC+ENR approach, *i.e.*, quantum coupled-channel calculations with the semiclassical relationships for the neutron transfer probabilities [59]. The neutron rearrangement in four PQ4NT systems ^{32}S+^{94,96}Zr and ^{40}Ca+^{94,96}Zr broadens the barrier distribution functions. The low-en-
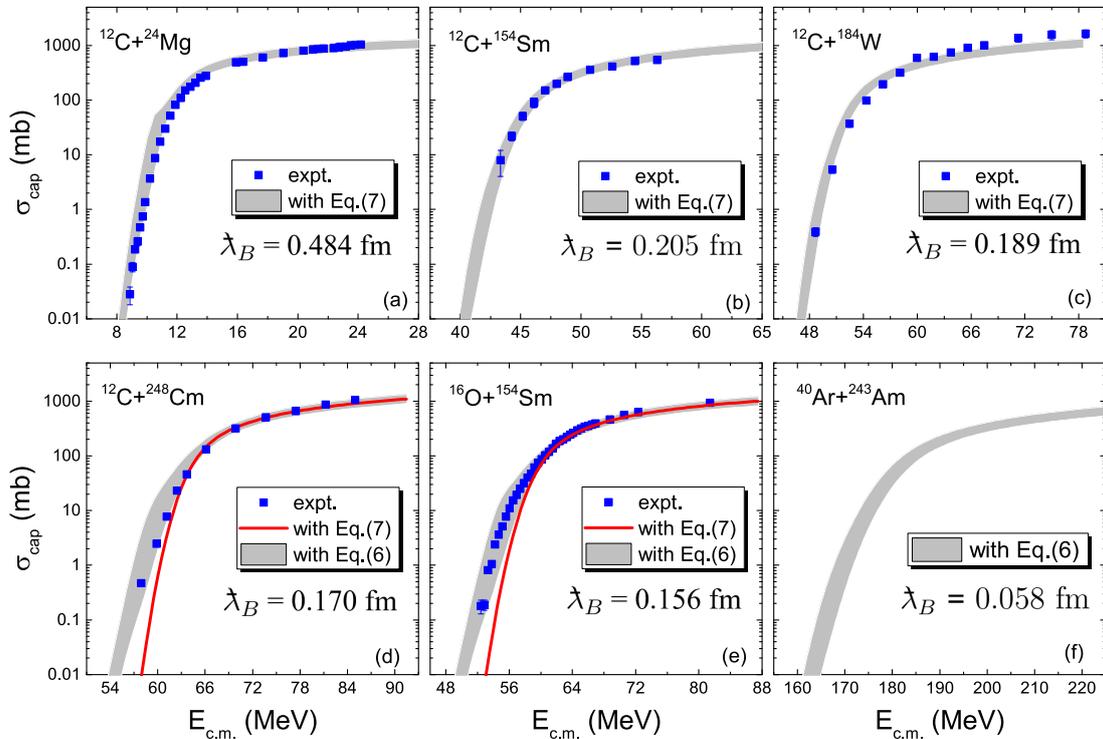
Fig. 7. (color online) Fusion excitation functions for six fusion reactions with deformed nuclei. The shadow represents the uncertainty of EBD2.2 predictions, and the squares represent the experimental data taken from Refs. [6, 54−58].

ergy tails (see Fig. 2 and Fig. 3 in [59]) caused by the neutron transfer significantly enhance the sub-barrier capture cross sections. In EBD2.2, PQ4NT lowers the average barrier height and widens the width of the barrier distribution when $Q_{4n} > 0$, which is in good agreement with the conclusions from QCC+ENR. Zagrebaev also noted that the neutron transfer effects in ^{40}Ca+^{48}Ca lower the most probable barrier height and widen the width of the barrier distribution [60]. In addition, neutron transfer is clearly observed from the improved quantum molecular dynamics simulations for ^{132}Sn+^{40}Ca, and the ratio of neutron-density to proton-density at the neck is higher than the N/Z of the compound nucleus by a factor of two when the reaction partners contact each other [29].

To further understand the effects of PQ4NT, we investigate the capture barrier height using the microscopic time-dependent Hartree-Fock (TDHF) theory. Based on the TDHF code Sky3D [61], the capture barrier heights V_B^{TDHF}[62] for the four groups of fusion reactions ^{40,48}Ca+^{48}Ca, ^{40,48}Ca+^{132}Sn, ^{40,48}Ca+^{208}Pb, and ^{40,48}Ca+^{96}Zr are calculated using the Skyrme energy density functional with the parameter set SLy6 [63]. Table 2 shows the calculated results, where V_{FD} represents the corresponding frozen-density barrier height obtained using the same Skyrme energy density functional with the extended Thomas-Fermi approach [64]. The values of Q_{4n} are presented for comparison. The TDHF calculations encompass a variety of microscopic effects including proton transfer, nucleon exchange, and collective excitations. The systematic reduction of $V_B^{\text{TDHF}}/V_{\text{FD}}$ for reactions with $Q_{4n} > 0$ compared with those with $Q_{4n} < 0$ indicates that the four-neutron transfer plays a significant role in lowering the dynamical barrier when it is energetically favorable. This observation aligns with the PQ4NT hypothesis that sustained neutron transfer facilitates barrier reduction. As indicated in Table 2, the values of Q_{4n} are positive for ^{40}Ca-induced reactions and those of Q_{4n} are negative for ^{48}Ca-induced reactions; further, the ratio

Table 2. Capture barrier heights for reactions with ^{40,48}Ca bombarding on nearly spherical nuclei.

Reaction	V_B^{TDHF} /MeV	V_{FD} /MeV	$V_B^{\text{TDHF}}/V_{\text{FD}}$	Q_{4n} /MeV
^{40}Ca+^{48}Ca	51.98	54.81	0.948	+3.87
^{40}Ca+^{96}Zr	95.07	101.53	0.936	+9.64
^{40}Ca+^{132}Sn	114.38	120.28	0.951	+13.44
^{40}Ca+^{208}Pb	176.91	185.51	0.954	+9.98
^{48}Ca+^{48}Ca	51.12	53.52	0.955	−12.72
^{48}Ca+^{96}Zr	93.51	99.32	0.942	−6.95
^{48}Ca+^{132}Sn	112.66	118.32	0.952	−3.14
^{48}Ca+^{208}Pb	174.78	182.32	0.959	−6.60

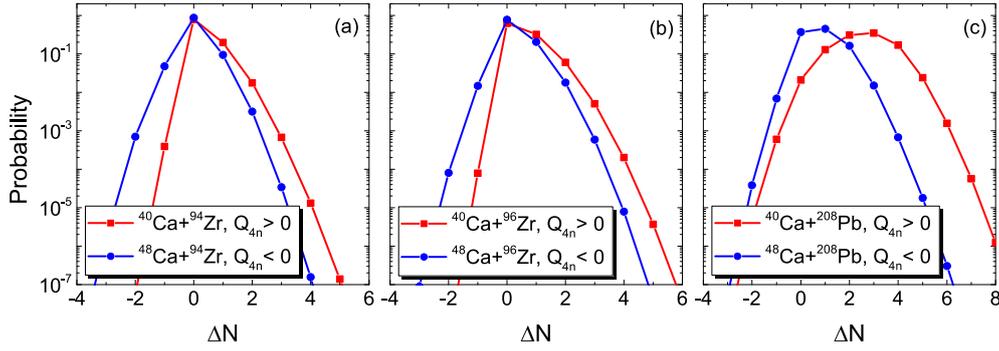$V_B^{\text{TDHF}}/V_{\text{FD}}$ in ^{40}Ca-induced reactions is systematically smaller than those in the ^{48}Ca-induced reactions. Thus, PQ4NT contributes significantly to the additional reduction of the dynamical barrier in these reactions.

In addition to the fusion barrier distribution directly extracted from the measured fusion excitation function, a similar barrier distribution can be extracted from quasi-elastic scattering (a sum of elastic, inelastic, and transfer processes) at backward angles [42, 65, 66]. The fusion and quasi-elastic scattering are related to each other because of the flux conservation, and therefore, similar information can be obtained from those processes. The similarity between the two representations for the barrier distribution has been shown to hold for some intermediate mass systems [65]. In this study, we also investigate the neutron transfer in the back-angle quasi-elastic scattering of ^{40,48}Ca+^{94,96}Zr and ^{40,48}Ca+^{208}Pb using the TDHF theory with the particle number projection approach [67, 68]. The incident energies in the calculations are set as $E_{\text{c.m.}}$ = 96.02 MeV, 93.55 MeV, 95.32 MeV, 93.13 MeV, 176.00 MeV, and 174.00 MeV for ^{40}Ca+^{94}Zr, ^{48}Ca+^{94}Zr, ^{40}Ca+^{96}Zr, ^{48}Ca+^{96}Zr, ^{40}Ca+^{208}Pb, and ^{48}Ca+^{208}Pb, respectively; these values are slightly lower than the corresponding capture thresholds. Figure 8 shows the transfer probability of neutrons transferred from target to projectile (ΔN), where $\Delta N > 0$ indicates neutrons being transferred from the target to the projectile and $\Delta N < 0$ indicates neutrons being transferred from the projectile to the target. As shown in Fig. 8, for systems with $Q_{4n} > 0$ (exothermic reactions), such as ^{40}Ca+^{94,96}Zr and ^{40}Ca+^{208}Pb, the probability at $\Delta N = 4$ is considerably higher than that for the corresponding systems with $Q_{4n} < 0$ (endothermic reactions). For example, the probability of ^{40}Ca+^{94}Zr at $\Delta N = 4$ is approximately 10^{-5}, while that of ^{48}Ca+^{94}Zr is only 10^{-7}. A higher probability for 4n transfer observed in the back-angle quasi-elastic scattering provides independent and direct microscopic evidence for the propensity of this multi-neutron process to occur as the nuclei approach the barrier. This propensity is fundamentally linked to the mechanism of neutron-rich neck formation, which subsequently lowers the dynamical fusion barrier.

PQ4NT influences the fusion barrier in two interrelated ways: lowering the average barrier height and broadening the barrier distribution. During the approach of the colliding nuclei, the transfer of four neutrons from the neutron-rich partner to the neutron-deficient one is energetically favorable when $Q_{4n} > 0$. This sustained neutron transfer leads to the formation of a neutron-rich neck between the nuclei, which reduces the Coulomb repulsion and thus the effective barrier height. Concurrently, the transfer process introduces additional degrees of freedom and dynamical fluctuations, which manifest as a wider barrier distribution. In the EBD2.2 parametrization, these effects are captured by the correction terms Δ_{tr} in both the average barrier height V_B and width W. The

Fig. 8. (color online) Neutron transfer probability as a function of the number of neutrons transferred from the target nucleus to the projectile nucleus in the back-angle quasi-elastic scattering of ^{40,48}Ca+^{94,96}Zr and ^{40,48}Ca+^{208}Pb. The squares and circles indicate the results for reactions with $Q_{4n} > 0$ and those with $Q_{4n} < 0$, respectively.

term $\Delta_{\text{tr}} = Q_{4n}|I_1 - I_2|/2$ quantifies the energy gain from the four-neutron transfer weighted by the isospin asymmetry difference, reflecting the propensity for neutron flow between the reaction partners. The inclusion of Δ_{tr} in W further accounts for the smearing of the barrier caused by the neutron transfer dynamics, which is consistent with the observed enhancement of the sub-barrier capture cross sections.

IV. SUMMARY

In this study, the effects of PQ4NT on sub-barrier capture cross sections were systematically examined within the EBD2 framework. For reactions with $Q_{4n} > 0$, such as ^{28}Si, ^{32}S+^{154}Sm, and ^{40}Ca+^{94,96}Zr, sustained neutron-pair transfer leads to a reduction in the fusion barrier height and a concomitant enhancement of capture cross sections at sub-barrier energies. In contrast, systems with positive Q_{2n} but negative Q_{4n}, which are exemplified by ^{18}O+^{58}Ni and ^{18}O+^{116}Sn, exhibit no discernible enhancement because neutron transfer ceases after the initial pairs. The original EBD2 model accurately reproduces experimental data for reactions with $Q_{4n} < 0$, including ^{16}O+^{154}Sm and ^{48}Ca+^{154}Sm. However, it systematically underestimates sub-barrier cross sections for reactions with $Q_{4n} > 0$. By incorporating the effects of PQ4NT through modifications to both the barrier height and distribution width, the predicted capture excitation functions for all 13 studied systems show significantly improved agreement with experimental data. Furthermore, TDHF calculations indicate greater dynamic barrier reduction in ^{40}Ca-induced reactions (with $Q_{4n} > 0$) compared to ^{48}Ca-induced ones, and considerably larger neutron pickup probabilities are observed in the quasi-elastic scattering reactions induced by ^{40}Ca. Predictions for as-yet unmeasured systems such as ^{36}Ar+^{208}Pb and ^{44}Ti+^{208}Pb suggest observable PQ4NT-induced enhancement. These results underscore the critical role of multi-neutron transfer continuity in sub-barrier fusion dynamics. The proposed model extensions yield a 20% reduction in cross-section deviation, demonstrating notable predictive improvement. We also quantified the predictive uncertainty of the model by deriving an energy-dependent RMSD. The uncertainties are within half an order of magnitude at sub-barrier energies and approximately 21.6% at energies well above the barrier.

DATA AVAILABILITY STATEMENT

Online calculations with EBD2.2 are available on http://www.imqmd.com/fusion/EBD2B.html

---

References

[1] C. Y. Wong, Phys. Rev. Lett. **31**, 766 (1973)
[2] R. Bass, Nucl. Phys. A **231**, 45 (1974)
[3] W. J. Swiatecki, Nucl. Phys. A **376**, 275 (1982)
[4] R. A. Broglia and A. Winther, *Heavy Ion Reactions*, Frontiers in Physics, Vol. **84** (Addison-Wesley, 1991)
[5] Rajeev K. Puri and Raj K. Gupta, Phys. Rev. C **45**, 1837 (1992)
[6] J. R. Leigh, M. Dasgupta, D. J. Hinde et al., Phys. Rev. C **52**, 3151 (1995)
[7] C. R. Morton, A. C. Berriman, M. Dasgupta et al., Phys. Rev. C **60**, 044608 (1999)
[8] C. L. Jiang, W. F. Henning, B. P. Kay et al., Phys. Rev. C **110**, L051604(2024)
[9] V. Yu. Denisov, Phys. Rev. C **109**, 044618 (2024)
[10] M.-H. Zhang et al., Phys. Rev. C **109**, 014622 (2024)
[11] R. G. Stokstad, Y. Eisen, S. Kaplanis et al., Phys. Rev. Lett. **41**, 465 (1978)
[12] M. Dasgupta, D. J. Hinde, N. Rowley et al., Annu. Rev. Nucl. Part. Sci. **48**, 401 (1998)
[13] R. Wolski, Phys. Rev. C **88**, 041603(R) (2013)
[14] H. M. Jia, C. J. Lin et al., Phys. Rev. C **90**, 031601(R) (2014)
[15] K. Hagino, N. Rowley, and A. T. Kruppa, Comput. Phys. Commun. **123**, 143 (1999)

[16] C. H. Dasso and S. Landowne, Comput. Phys. Commun. **46**, 187 (1987)
[17] V. V. Sargsyan, G. G. Adamian, N. V. Antonenko *et al.*, Phys. Rev. C **84**, 064614 (2011)
[18] H. M. Jia, C. J. Lin, F. Yang *et al.*, Phys. Rev. C **86**, 044621 (2012).
[19] V. A. Rachkov, A. V. Karpov, A. S. Denikin *et al.*, Phys. Rev. C **90**, 014614 (2014)
[20] G. L. Zhang, X. X. Liu, and C. J. Lin, Phys. Rev. C **89**, 054602 (2014)
[21] V. V. Sargsyan, G. G. Adamian, N. V. Antonenko *et al.*, Phys. Rev. C **91**, 014613 (2015)
[22] H. M. Jia *et al.*, Phys. Lett. B **755**, 43 (2016)
[23] A. M. Stefanini, G. Montagnoli, H. Esbensen *et al.*, Phys. Rev. C **96**, 014603 (2017)
[24] P.-W. Wen *et al.*, Chin. Phys. C **41**, 064102 (2017)
[25] B. Wang, K. Wen, W. J. Zhao *et al.*, At. Data Nucl. Data Tables **114**, 281 (2017)
[26] N. K. Deb *et al.*, Phys. Rev. C **102**, 034603 (2020)
[27] H. M. Jia *et al.*, Phys. Rev. C **111**, 034606 (2025)
[28] P. H. Stelson, Phys. Lett. B **205**, 190 (1988)
[29] N. Wang, L. Ou, Y. X. Zhan *et al.*, Phys. Rev. C **89**, 064601 (2014)
[30] P. Möller *et al.*, At. Data and Nucl. Data Tables **59**, 185 (1995)
[31] N. Wang, M. Liu, X. Z. Wu *et al.*, Phys. Lett. B **734**, 215 (2014)
[32] N. Wang, Chin. Phys. C **49**, 124106 (2025)
[33] K. Siwek-Wilczyńska and J. Wilczyński, Phys. Rev. C **69**, 024611 (2004)
[34] H. Lü, A. Marchix, Y. Abe *et al.*, Comp. Phys. Comm. **200**, 381 (2016)
[35] Q. Mo, M. Liu, and N. Wang, Phys. Rev. C **90**, 024320 (2014)
[36] M. Trotta *et al.*, Eur. Phys. J. A **25**, 615 (2005)
[37] S. Gil, D. Abriola, D. E. DiGregorio *et al.*, Phys. Rev. Lett. **65**, 3100 (1990)
[38] P. R. S. Gomes, I. C. Charret, R. Wanis *et al.*, Phys. Rev. C **49**, 245 (1994)
[39] V. Tripathi, L. T. Baby, J. J. Das *et al.*, Phys. Rev. C **65**, 014614 (2001)
[40] Y. Chen, H. Yao, M. Liu *et al.*, Atom. Data Nucl. Data Tables **154**, 101587 (2023)
[41] A. M. Stefanini, B. R. Behera, S. Beghini *et al.*, Phys. Rev. C **76**, 014610 (2007)
[42] H. Timmers, D. Ackermann, S. Beghini *et al.*, Nucl. Phys. A **633**, 421 (1998)
[43] F. Scarlassara, S. Beghini, G. Montagnoli *et al.*, Nucl. Phys. A **672**, 99 (2000)
[44] J. J. Kolata, A. Roberts, A. M. Howard *et al.*, Phys. Rev. C **85**, 054603 (2012)
[45] H. M. Jia, C. J. Lin, F. Yang *et al.*, Phys. Rev. C **89**, 064605 (2014)
[46] H. Q. Zhang, C. J. Lin, F. Yang *et al.*, Phys. Rev. C **82**, 054609 (2010)
[47] R. Pengo, D. Evers, K. E. G. Löbner *et al.*, Nucl. Phys. A **411**, 255 (1983)
[48] S. Misuoka, H. Ikezoe, K. Nishio *et al.*, Phys. Rev. C **62**, 054603 (2000)
[49] M. Dasgupta and D. J. Hinde, Nuc. Phys. A **734**, 148 (2004)
[50] D. J. Hinde, C. R. Moron, M. Dasgupta *et al.*, Nucl. Phys. A **592**, 271 (1995)
[51] K. Nishio, H. Ikezoe, I. Nishinaka *et al.*, Phys. Rev. C **82**, 044604 (2010)
[52] M. G. Itkis, G. N. Knyazheva, I. M. Itkisa *et al.*, Eur. Phys. J. A **58**, 178 (2022)
[53] J.-J. Li, J.-B. Tian, X.-R. Zhang *et al.*, Phys. Rev. C **112**, 064603 (2025)
[54] G. Montagnoli *et al.*, J. Phys. G: Nucl. Part. Phys. **49**, 095101 (2022)
[55] S. Gary and C. Volant, Phys. Rev. C **25**, 1877 (1982)
[56] S. Sanila *et al.*, Phys. Rev. C **106**, 024614 (2022)
[57] T. Banerjee *et al.*, Phys. Rev. C **102**, 024603 (2020)
[58] S. Gil *et al.*, Phys. Rev. C **31**, 1752 (1985)
[59] A. V. Karpov, V. A. Rachkov, and V. V. Samarin, Phys. Rev. C **92**, 064603 (2015)
[60] V. I. Zagrebaev, Phys. Rev. C **67**, 061601(R) (2003)
[61] J. A. Maruhn, P. G. Reinhard, P. D. Stevenson *et al.*, Comp. Phys. Comm. **185**, 2195 (2014)
[62] H. Yao, H. Yang, and N. Wang, Phys. Rev. C **110**, 014602 (2024)
[63] E. Chabanat, P. Bonche, P. Haensel *et al.*, Nucl. Phys. A **635**, 231 (1998)
[64] M. Liu, N. Wang, Z.-X. Li *et al.*, Nucl. Phys. A **768**, 80 (2006)
[65] M. Zamrun F. *et al.*, Phys. Rev. C **77**, 034604 (2008)
[66] H. Timmers *et al.*, Nucl. Phys. A **584**, 190 (1995)
[67] Z. Wu and L. Gao, Phys. Rev. C **100**, 014612 (2019)
[68] C. Simenel, Phys. Rev. Lett. **105**, 192701 (2010)